Photorecombination of highly charged uranium ions

M. S. Pindzola and F. J. Robicheaux
Department of Physics, Auburn University, Auburn, Alabama 36849

N. R. Badnell
Department of Physics, University of Strathclyde, Glasgow G4 0NG, Scotland

M. H. Chen
Department of Physics, Lawrence Livermore National Laboratory, Livermore, California 94551

M. Zimmermann
Department of Physics, University of Giessen, Giessen, Germany
(Received 6 February 1995)

Photorecombination cross sections for highly charged uranium ions are calculated using many-body perturbation theory. The cross sections are resolved with regard to the final recombined level, corresponding to different x-ray light emitted during radiative stabilization of the dielectronic capture resonances. Interference between the radiative and dielectronic recombination processes is found to be more important for the weaker x-ray-resolved partial photorecombination cross sections than for the total cross sections.

PACS number(s): 34.80.Kw

I. INTRODUCTION

Recent experimental observations [1–3] of photorecombination processes in highly charged ions have challenged our theoretical understanding of strong-field quantum electrodynamics. The energy positions of the observed resonance structures provide sensitive tests of Lamb shift calculations in multielectron systems [4]. Information on the detailed shape of the nuclear charge distribution may also be extracted from the resonance energies [5]. The cross section heights of the observed resonance features provide good tests of Auger rate calculations in which static, magnetic, and retardation effects need to be included in the electron-electron interaction [6–8]. Finally the detailed shape of the observed resonance structures provide tests of theoretical studies which include the quantum interference between the processes of radiative and dielectronic recombination [9,10].

In this paper we present total and partial photorecombination cross sections for highly charged uranium ions which include the interference between radiative and dielectronic recombination. The partial photorecombination cross sections are resolved as to the final state of the recombined ion and can be experimentally identified by the different x-ray light emitted during radiative stabilization of the dielectronic capture resonances. We find that although interference may have a small effect on the total cross sections, it can be important for some of the weaker x-ray resolved partial cross sections. This confirms the possibility that recent asymmetries seen in the x-ray resolved photorecombination spectra from a mixture of highly charged uranium ions [3] may be due to quantum interference. In Sec. II we outline the theory of interference between radiative and dielectronic recombination, in Sec. III we describe our fully relativistic Dirac-Fock numerical methods, in Sec. IV we present total and partial photorecombination cross sections for the $KL_{12}L_3$ resonances in U^{90+} and U^{88+}, and in Sec. V we conclude with a brief summary.

II. THEORY

In lowest-order perturbation theory the matrix element for the photoionization of an atomic ion is given by (in atomic units):

$$M(\alpha \to \beta) = \langle \psi_\beta | D | \psi_\alpha \rangle \ , \tag{1}$$

where $|\psi_\alpha\rangle$ is a bound state, $|\psi_\beta\rangle$ is a continuum state, and D is the radiation field interaction. The contribution from a single autoionizing resonance state $|\psi_n\rangle$, obtained by considering either bound-continuum configuration-interaction theory [11] or diagrammatic many-body perturbation theory [12], yields the following modified matrix element [13]:

$$M(\alpha \to \beta) = \langle \psi_\beta | D | \psi_\alpha \rangle \left(1 - \frac{i A_a(n \to \beta)/2}{\Delta + i\frac{\Gamma\eta}{2}} \right) + \frac{\langle \psi_\beta | V | \psi_n \rangle \langle \psi_n | D | \psi_\alpha \rangle}{\Delta + i\frac{\Gamma\eta}{2}} \ , \tag{2}$$

where $A_a(n \to \beta)$ is the autoionizing rate; V is the electron-electron interaction: Δ is the energy detuning from resonance, $\eta = 1 + \gamma/\Gamma$; γ is the total radiative width; and Γ is the total autoionizing width. It is convenient to define the line-profile function [11]

$$q_{\alpha\beta} = \frac{\langle \psi_\beta | V | \psi_n \rangle \langle \psi_n | D | \psi_\alpha \rangle}{\langle \psi_\beta | D | \psi_\alpha \rangle (A_a(n \to \beta)/2)} \tag{3}$$

and recast Eq. (2) in the form

$$M(\alpha \to \beta) = \langle \psi_\beta | D | \psi_\alpha \rangle \left(\frac{\zeta + q_{\alpha\beta} A_a(n \to \beta)/\Gamma + i\eta - iA_a(n \to \beta)/\Gamma}{\zeta + i\eta} \right) , \tag{4}$$

where $\zeta = \Delta/\frac{\Gamma}{2}$.

Further perturbation theory terms may be incorporated into the matrix element for photoionization utilizing a projection-operator formalism [14]. The further modified matrix element is given by

$$M(\alpha \to \beta) = \langle \psi_\beta | D | \psi_\alpha \rangle \left(\frac{\zeta + q_{\alpha\beta} A_a(n \to \beta)/\Gamma + i\eta - i\sum_{\beta'} \frac{q_{\beta\alpha} A_a(n \to \beta)}{q_{\beta'\alpha}\Gamma} - i\sum_{\alpha'} \frac{q_{\beta\alpha} A_r(n \to \alpha')}{q_{\beta\alpha'}\Gamma}}{\zeta + i\eta + i\eta' - 2\sum_{\alpha\beta} \frac{A_r(n \to \alpha)}{q_{\beta\alpha}\Gamma}} \right) , \tag{5}$$

where

$$\eta' = \sum_{\alpha\alpha'\beta} \frac{A_r(n \to \alpha') A_r(n \to \alpha)}{q_{\beta\alpha'}\Gamma^2} \left(\frac{1}{q_{\beta\alpha'}} - \frac{1}{q_{\beta\alpha}} \right) + \sum_{\alpha\beta} \frac{A_r(n \to \alpha)}{q_{\beta\alpha}} \left(\frac{1}{q_{\beta\alpha} A_a(n \to \beta)} - \sum_{\beta'} \frac{1}{q_{\beta'\alpha}\Gamma} \right) , \tag{6}$$

and $A_r(n \to \alpha)$ is the radiative rate.

The electric-dipole photoionization cross section for an atomic ion is given by

$$\sigma_{PI} = \frac{8\pi c}{3\omega p} |M(\alpha \to \beta)|^2 , \tag{7}$$

where ω is the frequency of the radiation field, c is the speed of light, $p = \sqrt{2\epsilon + \frac{\epsilon^2}{c^2}}$ is the photoelectron linear momentum, ϵ is the total energy of the photoelectron minus its rest energy, and the continuum normalization is $\sqrt{1 + \frac{\epsilon}{2c^2}}$ times a sine function. With the aid of the principle of detailed balance, the electric-dipole photorecombination cross section for an atomic ion is given by

$$\sigma_{PR} = \frac{8\pi\omega}{3cp^3} |M(\beta \to \alpha)|^2 . \tag{8}$$

We note that for level to level photorecombination one must multiply Eq. (8) by the additional factor of (g_α/g_β), where g_β is the statistical weight of level β in the target ion and g_α is the statistical weight of level α in the final recombined ion.

For all of the photorecombination cross sections reported in this paper, we found no significant difference between employing either the matrix element of Eq. (4) or the matrix element of Eq. (5). The last term in the numerator of Eq. (4) originates in the third order of perturbation theory and should be the most important term in that order. The additional terms found in both the numerator and denominator of Eq. (5) originate in both the third order and fourth order of perturbation theory.

III. NUMERICAL METHODS

The photorecombination cross sections for highly charged uranium ions are calculated within a fully relativistic Dirac-Fock approach. Resonance energies and bound-state orbitals are obtained using a multiconfiguration Dirac-Fock-Breit atomic structure code [15–17]. Additional QED corrections are made to the resonance energies. The continuum-state orbitals are solutions to the single-channel Dirac equation, where the scattering potential is the sum of the nuclear potential and a distorting potential constructed from previously calculated bound orbitals for the target.

The electric-dipole radiative rates found in Eqs. (2)–(6) are given by

$$A_r(\alpha \to \beta) = \frac{4\omega}{3c} (M_{\alpha\beta})^2 , \tag{9}$$

where

$$M_{\alpha\beta} = \sum_i \sum_j c_i^\alpha c_j^\beta d_{ij}^{\alpha\beta} \langle a || m || b \rangle , \tag{10}$$

the c_i^α are the subconfiguration mixing coefficients for the atomic state α, and the $d_{ij}^{\alpha\beta}$ are the electric-dipole angular coefficients between subconfigurations provided by a relativistic tensor operator code [18]. The reduced matrix element of Eq. (10) is given by

$$\langle a || m || b \rangle = (-1)^{j_a - \frac{1}{2}} \sqrt{2j_b + 1} \begin{pmatrix} j_b & 1 & j_a \\ \frac{1}{2} & 0 & -\frac{1}{2} \end{pmatrix} T_{ab}(r) , \tag{11}$$

where j_a is the total angular momentum of orbital a, and the usual notation for a $3j$ symbol is employed. In the Coulomb (velocity) gauge the radial function of Eq. (11) is given by

$$T_{ab}(r) = \frac{1}{2}(\kappa_a - \kappa_b) I_2^+(r) + I_2^-(r) - (\kappa_a - \kappa_b) I_0^+(r) + I_0^-(r) , \tag{12}$$

where

$$I_\lambda^\pm(r) = \int_0^\infty (P_a Q_b \pm Q_a P_b) j_\lambda \left(\frac{\omega r}{c} \right) dr , \tag{13}$$

P_a is the large component radial wave function for the orbital a, Q_a is the small component radial wave function for the orbital a, j_λ is a spherical Bessel function,

$\kappa_a = -2(j_a - \ell_a)(j_a + \frac{1}{2})$, and ℓ_a is the orbital angular momentum of orbital a. In the nonrelativistic limit

$$T_{ab}(r) = -\frac{1}{c}\int_0^\infty P_b \left(\frac{d}{dr} + \frac{\ell_a(\ell_a+1) - \ell_b(\ell_b+1)}{2r}\right) \times P_a dr \ . \tag{14}$$

Expressions for radial functions similar to Eqs. (12)–(13) were also derived in the Babushkin (length) gauge.

The autoionizing rates found in Eqs. (2)–(6) are given by

$$A_a(\alpha \to \beta) = \frac{4}{p}(M_{\alpha\beta})^2 \ , \tag{15}$$

where

$$M_{\alpha\beta} = \sum_i \sum_j \sum_\lambda c_i^\alpha c_j^\beta a_{ij\lambda}^{\alpha\beta} \langle ab|m_\lambda|cd\rangle \ , \tag{16}$$

and $a_{ij\lambda}^{\alpha\beta}$ are the multipolar angular coefficients between subconfigurations provided by a relativistic Coulomb algebra code [19] and a relativistic Breit algebra code [16]. The matrix element of Eq. (16) for the electrostatic interaction between electrons is given by

$$\langle ab|m_\lambda|cd\rangle = \int_0^\infty \int_0^\infty (P_a P_b + Q_a Q_b) \times (P_c P_d + Q_c Q_d) \frac{r_<^\lambda}{r_>^{\lambda+1}} dr_1 dr_2 \ . \tag{17}$$

Expressions for matrix elements similar to Eq. (17) were also derived for the retarded electromagnetic interaction between electrons.

Besides rates, various matrix elements between bound, resonance, and continuum states are needed for the complete evaluation of the photorecombination cross section of Eq. (8) via either Eq. (4) or Eq. (5). Our organizational procedure involves generating lists of bound-resonance radiative rates, resonance-continuum autoionizing rates, and bound-continuum photoionization cross sections which include the signs of all matrix elements. It is important that the direction of the matrix element evaluation in the direct contribution is the same as that used in the indirect contribution.

IV. RESULTS

The following direct (radiative recombination) pathways contribute to the total photorecombination cross section for U^{90+} in the vicinity of the $KL_{12}L_3$ resonances:

$$\begin{aligned} e^- + U^{90+}(1s^2) &\to U^{89+}(1s^2 2s) + \omega_1 \ , \\ e^- + U^{90+}(1s^2) &\to U^{89+}(1s^2 2\bar{p}) + \omega_1 \ , \\ e^- + U^{90+}(1s^2) &\to U^{89+}(1s^2 2p) + \omega_2 \ , \end{aligned} \tag{18}$$

where $\omega_1 \approx 100$ keV and $\omega_2 \approx 95$ keV. The following indirect (dielectronic recombination) pathways are the dominant contribution to the total cross section:

$$\begin{aligned} e^- + U^{90+}(1s^2) &\to U^{89+}(1s2s2p) \to U^{89+}(1s^2 2s) + \omega_1, \\ e^- + U^{90+}(1s^2) &\to U^{89+}(1s2\bar{p}2p) \to U^{89+}(1s^2 2\bar{p}) + \omega_1 \ , \\ e^- + U^{90+}(1s^2) &\to U^{89+}(1s2\bar{p}2p) \\ &\to U^{89+}(1s^2 2p) + \omega_2 \ . \end{aligned} \tag{19}$$

In Table I we present the energies and the $1s^2$ autoionizing rates for the eight possible levels in the $1s2s2p$ and $1s2\bar{p}2p$ subconfigurations. In Fig. 1 we present the total photorecombination cross section for the $KL_{12}L_3$ resonances in U^{90+}. The solid curve includes interference between radiative and dielectronic recombination via Eqs. (4) or (5), while the dashed curve neglects the quantum interference between the two processes. The heights of the resonance features are generally proportional to the $1s^2$ autoionizing rates found in Table I, while the widths are proportional to the much stronger radiative rates. There are four strong resonance features in the total cross section due to the $1s2\bar{p}(1)2p(j = 5/2)$, $1s2\bar{p}(1)2p(j = 3/2)$, $1s2s(0)2p(j = 3/2)$, and $1s2\bar{p}(0)2p(j = 3/2)$ levels. As stated previously [10], although quantum interference effects are noticeable in the line shapes, the integrated cross sections are much less affected.

In Fig. 2 we present the partial photorecombination cross section into the $1s^2 2s(j = 1/2)$ and $1s^2 2\bar{p}(j = 1/2)$ final recombined levels resulting in the emission of 100 keV x-ray light. The contribution from the $1s2\bar{p}(1)2p(j = 5/2)$ resonance has disappeared since it cannot dipole radiate to the $j = 1/2$ levels. Inclusion of $M2$ radiative transitions could restore some of its strength. In Fig. 3 we present the partial photorecombination cross section into the $1s^2 2p(j = 3/2)$ final recombined level resulting in the emission of 95 keV x-ray light. The contribution from the $1s2s(0)2p(j = 3/2)$

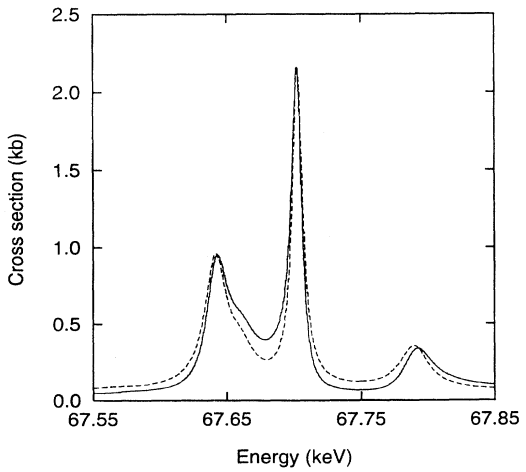

FIG. 1. Total photorecombination cross section for U^{90+} in the vicinity of the $KL_{12}L_3$ resonances. Solid curve—with quantum interference; dashed curve—without quantum inteference.

TABLE I. Energies and $1s^2$ autoionizing rates for the U^{89+} $KL_{12}L_3$ resonances.

Level	Energy (keV)	Rate (Hz)
$1s2s(1)2p(j=5/2)$	67.370	9.44×10^{11}
$1s2s(1)2p(j=3/2)$	67.489	2.61×10^{12}
$1s2s(1)2p(j=1/2)$	67.565	2.36×10^{12}
$1s2\bar{p}(1)2p(j=5/2)$	67.641	1.12×10^{14}
$1s2\bar{p}(1)2p(j=3/2)$	67.659	5.72×10^{13}
$1s2\bar{p}(1)2p(j=1/2)$	67.697	1.70×10^{13}
$1s2s(0)2p(j=3/2)$	67.702	2.04×10^{14}
$1s2\bar{p}(0)2p(j=3/2)$	67.789	7.68×10^{13}

resonance has disappeared since it cannot dipole radiate to the $j = 3/2$ level because they have the same parity. Inclusion of $M1$ or $E2$ radiative transitions could restore some of its strength. We note that due to propensity rules the $1s2\bar{p}(0)2p(j=3/2)$ resonance has a 20 times stronger probability for radiative decay to the $1s^2 2\bar{p}(j=1/2)$ level as to the $1s^2 2p(j=3/2)$ level, and thus it appears as a stronger feature in Fig. 2 than Fig. 3.

The following direct (radiative recombination) pathways contribute to the total photorecombination cross section for U^{88+} in the vicinity of the $KL_{12}L_3$ resonances:

$$\begin{aligned} e^- + U^{88+}(1s^2 2s^2) &\rightarrow U^{87+}(1s^2 2s^2 2\bar{p}) + \omega_1 , \\ e^- + U^{88+}(1s^2 2s^2) &\rightarrow U^{87+}(1s^2 2s^2 2p) + \omega_2 . \end{aligned} \tag{20}$$

The following indirect (dielectronic recombination) pathways are the dominant contribution to the total cross section:

$$\begin{aligned} e^- + U^{88+}(1s^2 2s^2) &\rightarrow U^{87+}(1s2s^2 2\bar{p}2p) \\ &\rightarrow U^{87+}(1s^2 2s^2 2\bar{p}) + \omega_1 \end{aligned} \tag{21}$$

$$\begin{aligned} e^- + U^{88+}(1s^2 2s^2) &\rightarrow U^{87+}(1s2s^2 2\bar{p}2p) \\ &\rightarrow U^{87+}(1s^2 2s^2 2p) + \omega_2 . \end{aligned}$$

TABLE II. Energies and $1s^2 2s^2$ autoionizing rates for the U^{87+} $KL_{12}L_3$ resonances.

Level	Energy (keV)	Rate (Hz)
$1s2s^2 2\bar{p}(1)2p(j=5/2)$	68.129	1.10×10^{14}
$1s2s^2 2\bar{p}(1)2p(j=3/2)$	68.147	5.56×10^{13}
$1s2s^2 2\bar{p}(1)2p(j=1/2)$	68.184	1.63×10^{13}
$1s2s^2 2\bar{p}(0)2p(j=3/2)$	68.274	7.60×10^{13}

In Table II we present the energies and $1s^2 2s^2$ autoionizing rates for the four possible levels in the $1s2s^2 2\bar{p}2p$ subconfiguration. The resonances associated with the $1s2s2\bar{p}^2 2p$ subconfiguration are also in the same energy range, but are not accessible from the $1s^2 2s^2$ ground state. The $1s2s^2 2\bar{p}2p$ resonances may autoionize to the $1s^2 2s2\bar{p}$ and $1s^2 2\bar{p}2p$ subconfigurations of U^{88+} and thus contribute to the overall autoionizing width Γ. The overall radiative width γ is again much larger than Γ. In Fig. 4 we present the total photorecombination cross section for the $KL_{12}L_3$ resonances in U^{88+}. Again the solid curve includes the interference between radiative and dielectronic recombination via Eqs. (4) or (5), while the dashed curve neglects the quantum interference between the two processes. There are three strong resonance features in the total cross section due to the $1s2s^2 2\bar{p}(1)2p(j=5/2)$, $1s2s^2 2\bar{p}(1)2p(j=3/2)$, and $1s2s^2 2\bar{p}(0)2p(j=3/2)$ levels.

In Fig. 5 we present the partial photorecombination cross section into the $1s^2 2s^2 2\bar{p}(j=1/2)$ final recombined level resulting in the emission of 100 keV x-ray light. The contribution from the $1s2s^2 2\bar{p}(1)2p(j=5/2)$ resonance has disappeared since it cannot dipole radiate, although some of its strength could be restored by inclusion of M2 radiation. In Fig. 6 we present the partial photorecombination cross section into the $1s^2 2s^2 2p(j=3/2)$ final recombined level resulting in the emission of 95 keV x-ray light. The contribution from all the strong resonances

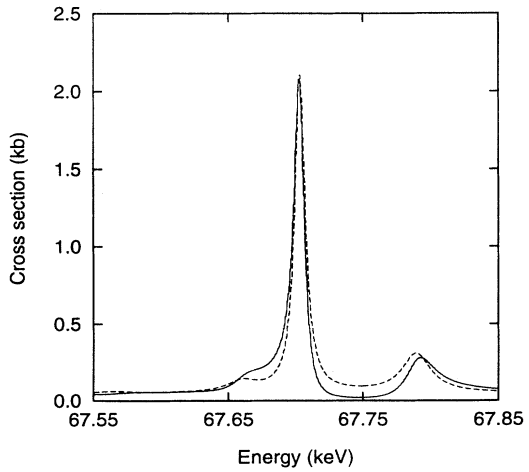

FIG. 2. Partial photorecombination cross section for U^{90+} in the vicinity of the $KL_{12}L_3$ resonances corresponding to emission of 100 keV x-ray light into the $1s^2 2s$ and $1s^2 2\bar{p}$ states of U^{89+}. Solid curve—with quantum interference; dashed curve—without quantum interference.

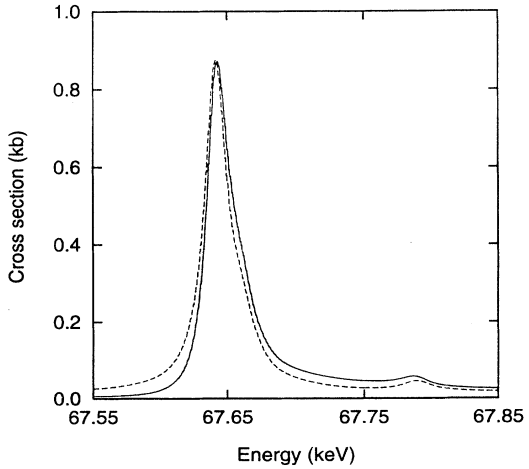

FIG. 3. Partial photorecombination cross section for U^{90+} in the vicinity of the $KL_{12}L_3$ resonances corresponding to emission of 95 keV x-ray light into the $1s^2 2p$ state of U^{89+}. Solid curve—with quantum interference; dashed curve—without quantum interference.

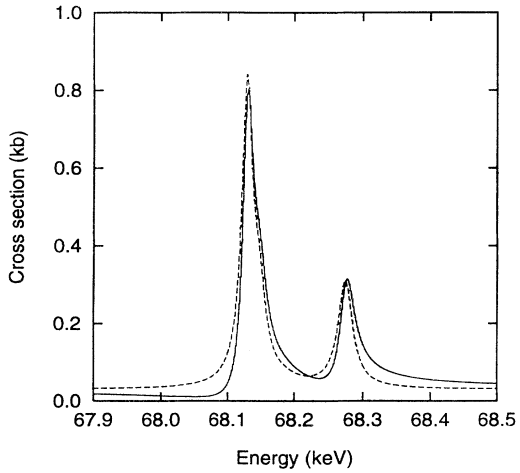

FIG. 4. Total photorecombination cross section for U^{88+} in the vicinity of the $KL_{12}L_3$ resonances. Solid curve—with quantum interference; dashed curve—without quantum interference.

in the total cross section are still present in this partial cross section.

The U^{88+} partial photorecombination cross section into the $1s^22s^22\bar{p}(j = 1/2)$ final recombined level, shown in Fig. 5, shows the largest degree of asymmetry due to quantum interference of the four partial cross sections presented in this section. A single continuum $[1s^22s^2\epsilon\bar{d}(j = 3/2)]$ may either directly recombine radiatively or indirectly recombine through the two $j = 3/2$ levels of the $1s2s^22\bar{p}2p$ subconfiguration. The total width of each resonance is approximately 4.0×10^{16} Hz. We note that the largest degree of asymmetry seen in the recent photorecombination experiment with uranium [3] is found for 100 keV light emission from the $KL_{12}L_3$ resonances (see their Fig. 3). The most abundant ions in the experiment were U^{88+} and U^{87+}.

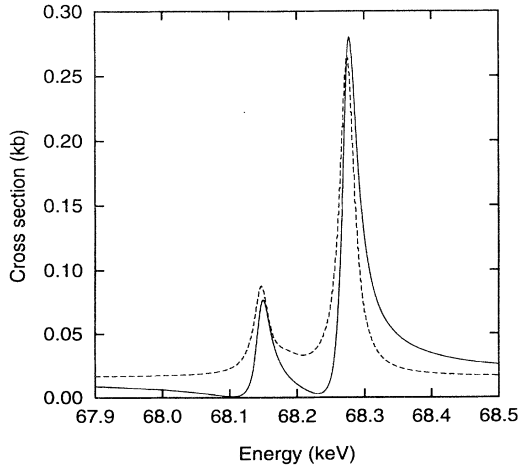

FIG. 5. Partial photorecombination cross section for U^{88+} in the vicinity of the $KL_{12}L_3$ resonances corresponding to emission of 100 keV x-ray light into the $1s^22s^22\bar{p}$ state of U^{87+}. Solid curve—with quantum interference; dashed curve—without quantum interference.

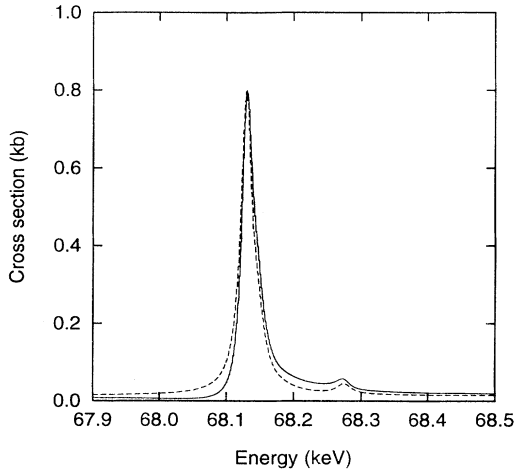

FIG. 6. Partial photorecombination cross section for U^{88+} in the vicinity of the $KL_{12}L_3$ resonances corresponding to emission of 95 keV x-ray light into the $1s^22s^22p$ state of U^{87+}. Solid curve—with quantum interference; dashed curve—without quantum interference.

V. SUMMARY

Using many-body perturbation theory we calculated the total and partial photorecombination cross sections for the ground states of both U^{90+} and U^{88+} in the vicinity of the $KL_{12}L_3$ resonances. We found no significant difference between cross sections calculated using the third-order matrix element expression of Eq. (4) and the fourth-order matrix element expression of Eq. (5) for the two ions. Quantum interference effects between the radiative and dielectronic recombination processes was found to be largest for the U^{88+} partial photorecombination cross section into the $1s^22s^22\bar{p}(j = 1/2)$ final recombined level. This particular partial cross section may serve as a convenient focus for future experiments which resolve on both x rays and charge state of the ion.

Through perturbation theory the positions of the resonances were determined using multiconfiguration Dirac-Fock-Breit atomic structure codes, with additional QED and nuclear volume corrections. We found that one needs to include static, magnetic, and retardation effects in the calculation of Auger rates and their associated matrix elements. Although we used a general relativistic multipole expansion to calculate radiative rates and their associated matrix elements, we limited ourselves in this paper to $E1$ radiation. As pointed out in Sec. IV, several resonances excluded by $E1$ selection rules may reappear in the partial cross sections when non-$E1$ multipole radiation is taken into account. The background radiative recombination process may be further enhanced by as much as 30% when higher-order multipoles are included. Besides including the interference between the resonances and their background, we also included interacting resonance effects by means of direct configuration-interaction; as for example between the two ($j = 3/2$)

levels in the $1s2s^22\bar{p}2p$ subconfiguration. Further interactions between resonances through the adjacent continuum [20] may also be handled in many-body perturbation theory.

ACKNOWLEDGMENTS

We would like to thank Professor D. C. Griffin of Rollins College and Dr. T. W. Gorczyca of Auburn University for several useful discussions. This work was supported in part by the U.S. Department of Energy under Grant No. DE-FG05-86-ER53217 with Auburn University, by an NSF Young Investigator Grant with Auburn University, by an EPSRC Grant No. GR K14346 with the University of Strathclyde, by the U.S. Department of Energy under Contract No. W-7405-ENG-48 with LLNL, and by a German Academic Exchange Service Grant.

[1] W. G. Graham, K. H. Berkner, E. M. Bernstein, M. W. Clark, B. Feinberg, M. A. McMahan, T. J. Morgan, W. Rathbun, A. S. Schlachter, and J. A. Tanis, Phys. Rev. Lett. **65**, 2773 (1990).

[2] W. Spies, A. Muller, J. Linkemann, A. Frank, M. Wagner, C. Kozhuharov, B. Franzke, K. Beckert, F. Bosch, H. Eickhoff, M. Jung, O. Klepper, W. Konig, P. H. Mokler, R. Moshammer, F. Nolden, U. Schaaf, P. Spadtke, M. Steck, P. Zimmerer, N. Grun, W. Scheid, M. S. Pindzola, and N. R. Badnell, Phys. Rev. Lett. **69**, 2768 (1992).

[3] D. A. Knapp, P. Beiersdorfer, M. H. Chen, J. H. Scofield, and D. Schneider, Phys. Rev. Lett. **74**, 54 (1995).

[4] S. A. Blundell, P. J. Mohr, W. R. Johnson, and J. Sapirstein, Phys. Rev. A **48**, 2615 (1993).

[5] G. Plunien, B. Muller, W. Greiner, and G. Soff, Phys. Rev. A **39**, 5428 (1989).

[6] M. H. Chen, Phys. Rev. A **41**, 4102 (1990).

[7] P. Zimmerer, N. Grun, and W. Scheid, Phys. Lett. A **148**, 457 (1990).

[8] M. S. Pindzola and N. R. Badnell, Phys. Rev. A **42**, 6526 (1990).

[9] V. V. Karasiev, L. N. Labzowsky, A. V. Nefiodov, and V. M. Shabaev, Phys. Lett. A **161**, 453 (1992).

[10] N. R. Badnell and M. S. Pindzola, Phys. Rev. A **45**, 2820 (1992).

[11] U. Fano, Phys. Rev. **124**, 1866 (1961).

[12] H. P. Kelly and R. L. Simons, Phys. Rev. Lett. **30**, 529 (1975).

[13] F. J. Robicheaux, T. W. Gorczyca, M. S. Pindzola, and N. R. Badnell, Phys. Rev. A (to be published).

[14] S. L. Haan and V. L. Jacobs, Phys. Rev. A **40**, 80 (1989).

[15] I. P. Grant, B. J. McKenzie, P. H. Norrington, D. F. Mayers, and N. C. Pyper, Comput. Phys. Commun. **21**, 207 (1980).

[16] B. J. McKenzie, I. P. Grant, and P. H. Norrington, Comput. Phys. Commun. **21**, 233 (1980).

[17] K. G. Dyall, I. P. Grant, C. T. Johnson, F. A. Parpia, and E. P. Plummer, Comput. Phys. Commun. **55**, 425 (1989).

[18] N. C. Pyper, I. P. Grant, and N. Beatham, Comput. Phys. Commun. **15**, 387 (1978).

[19] I. P. Grant, Comput. Phys. Commun. **5**, 263 (1973).

[20] M. S. Pindzola, N. R. Badnell, and D. C. Griffin, Phys. Rev. A **46**, 5725 (1992).